Settlement Prediction of a RAP-Supported Footing in Liquefiable Soils Subjected to a Seismic Loading

Tat Shing Thum[1]; Alba Yerro[2]; Russell A. Green[3]; Evin Ye[4]; Angela Saade[5]; and Kord Wissmann[6]

[1]Condon-Johnson & Associates, Inc. Email: TShingThum@condon-johnson.com
[2]Dept. of Civil and Environmental Engineering, Virginia Tech. Email: ayerro@vt.edu
[3]Dept. of Civil and Environmental Engineering, Virginia Tech. Email: rugreen@vt.edu
[4]Langan. Email: Eye@langan.com
[5]Gannett Fleming. Email: Asaade@gfnet.com
[6]Geopier Foundation Company. Email: KWissmann@geopier.com

ABSTRACT

Over the past 50 years, seismically induced soil liquefaction has resulted in billions of dollars of damage to structures. Recent examples include extensive damage to infrastructure in Haiti (2010), Christchurch, New Zealand (2010–2011), and Ecuador (2016), among many others. New structures may be constructed on soil enhanced by ground improvement such as compaction grouting, stone columns, or Rammed aggregate pier (RAP) systems that rely on soil densification and reinforcement to provide stability. In New Zealand, RAP systems have been subjected to extensive testing to demonstrate their veracity in providing a reinforced crust of soil below shallow foundations. The results of the testing have been used to formulate design guidance for a variety of structural classifications and to provide validation of numerical models used to simulate the seismic response of these foundations. This paper extends the knowledgebase about RAP-supported foundation behavior by presenting the results of fully coupled hydro-mechanical numerical models developed to estimate the support mechanisms important for stability and settlements. The results of the research indicate that RAP can significantly reduce the seismically induced settlement.

INTRODUCTION

Liquefaction has resulted in damage to the built environment in most major earthquakes. For example, during the 2010-2011 Canterbury Earthquake Sequence (CES) in New Zealand (Cubrinovski and Green 2010; Curbrinovski et al. 2011), damages amounting to NZ$40 billion were reported, with about half being attributed to liquefaction. New structures built in liquefaction-prone areas often require expensive pile foundations designed to bypass liquefiable soils. Alternatively, performing shallow ground improvement to create a non-liquefiable crust has been shown to be an effective alternative (Ishihara 1985; Green et al. 2018). In particular, densification-based methods are commonly used to compact loose to medium dense granular soils that are prone to liquefaction (Tonkin and Taylor 2015; Shahir and Ayoubi 2016). Although the effectiveness of ground improvement methods for densifying granular materials has been extensively documented, the effectiveness of columnar-supported foundations installed on reinforced soil profiles is not well understood.

In response to the 2010-2011 CES, a large-scale field test program known as the Ground Improvement Programme (GIP) was initiated by the New Zealand Earthquake Commission

(EQC) to evaluate the capability of eight shallow ground improvement methods in reducing risk due to liquefaction at a feasible cost and effort (Roberts 2017). Among the ground improvement methods tested, Roberts (2017) concluded that the 4-m deep RAP elements were a very competitive approach for creating a non-liquefiable crust.

This study focuses on the analysis of RAP-supported foundations. This ground improvement technique densifies the ground by first displacing the soil with a mandrel forming a cavity, and then filling the cavity with crushed gravel that is compacted to create dense, stiff, aggregate pier elements (Wissmann et al. 2015). The installation process increases the lateral stress in the surrounding soils that then couples the RAP element with the soil. This paper studies the co-seismic and post-seismic settlement of a 3-m-wide footing founded on RAP elements analyzed using a finite-difference framework. One of the keys and unique aspects of this study is that the numerical model of the subsurface is calibrated using the extensive field test data collected from the GIP (Thum et al. 2021). For the purpose of evaluating the importance of different improvement mechanisms, four different ground conditions are modeled, representing different levels of soil reinforcement. In the following, a description of the numerical model, subsurface conditions, and loading sequence are presented. Finally, the results are presented and discussed.

MODELING SUBSURFACE CONDITIONS AND LOADING SEQUENCE

The settlement of a 3-m-wide footing is investigated under the four subsurface conditions shown in Figure 1: natural soil (Model 1); natural soil reinforced with a densified zone of soil (Model 2); natural soil that has not been densified but is reinforced with two RAP elements (Model 3); and natural soil reinforced with two RAP elements surrounded by a zone of densified soil (Model 4). Models 2 and 3 are included in the analysis to investigate the effects of soil densification and RAP elements separately. As stated in the Introduction, the characteristics of the soil profile being modeled were determined from the extensive in-situ test data from Site 6 of the GIP (Roberts 2017). The upper 10 m of the profile is modeled using seven distinct layers, as shown in Figure 2. From the profile surface downwards, the profile is comprised of a shallow silty to poorly graded sand, a silt layer, a low to medium density fine silty sand, and a thick medium to dense well-graded clean sand layer (Table 1).

Fully-coupled hydro-mechanical plane strain analyses are performed using the commercial software FLAC2D configured for large strain and dynamic formulation. The model dimensions are 10 m high and 50 m wide, and a computational mesh of 0.25-m-square elements is used across the domain. The soils are modeled using the PM4Sand constitutive model, which was developed to predict the stress-strain response of soil under cyclic loading, including liquefaction problems (Boulanger and Ziotopoulou 2017). The densified soil is assumed to have a relative density (Dr) of 75%, which is in the mid-range of what can be reasonably achieved from the installation of RAPs. The RAP elements are compacted crushed gravel and for simplification, they are modeled as linear elastic materials. Note that this simplification could result in the presence of unrealistic tensile forces within the RAPs, but for the models analyzed in this study, no tensile stresses were observed in the RAPs throughout the calculation. The elastic properties are obtained by calibrating Models 1 and 4 with T-Rex data (Table 2). Although the use of a plane strain model to represent the RAP elements is a geometric simplification, the errors made by representing a 3D system in 2D space are partially nullified because the RAP width has been reduced to account for this effect. The equivalent RAP panel width was determined using methods proposed by Papadimitrious et al. (2006) for an equivalent moment of inertia.

All models are analyzed with and without a vertical load imposed on a footing. The footing is represented by a thin and weightless rigid beam, in which rocking is not allowed. Note that when the vertical load is applied, the inertial loading due to a theoretical superstructure is not considered. The reason for this simplification is that induced shear stresses due to inertial loading are dependent on the fundamental period of the structure, and the purpose of this paper is to present a reference scenario for future studies, in which the kinematic response of the superstructure is known. The stresses are initialized with elastic gravity loading assuming that the at-rest lateral earth pressure coefficient (K_o) is equal to 0.5. Next, for the models with the loaded footing, a static vertical load (240 kPa) representing the weight of a hypothetical superstructure is applied to the footing and numerically solved for quasistatic equilibrium. Thereafter, the models are subjected to the bottom-up dynamic loading. The ground motion used in the analyses was recorded at the North New Brighton School (NNBS) station during 2010, M_w7.1 Darfield earthquake (Bradley 2012). The duration of the acceleration time history is truncated using a minimum acceleration of 0.005g. Finally, the loading sequence of the analyses is concluded with a consolidation stage to allow for the dissipation of excess pore pressures (Δu) generated during the dynamic loading.

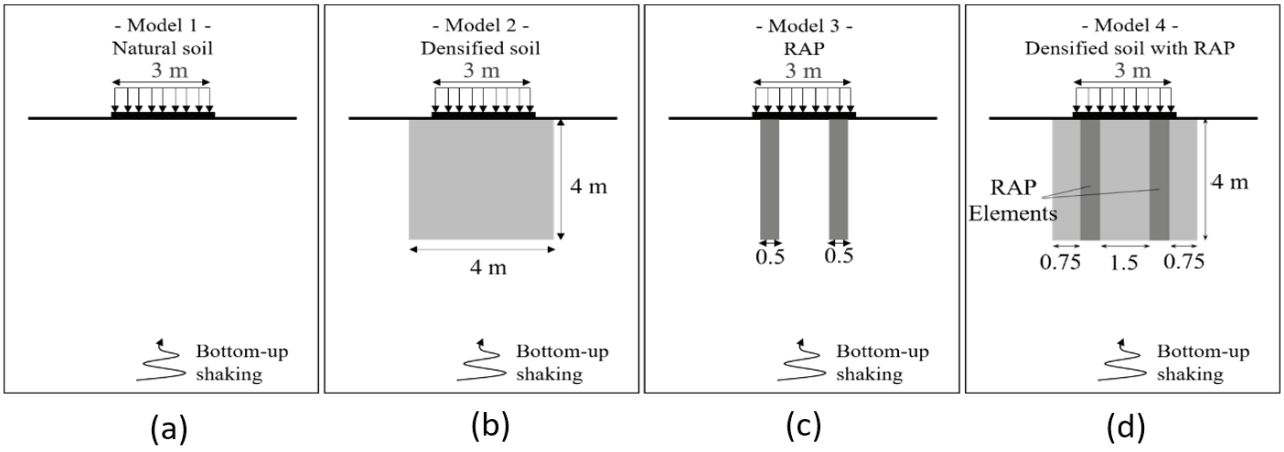

Figure 1. Model configurations (not to scale): (a) Model 1; (b) Model 2; (c) Model 3; and (d) Model 4. Soil layers not shown.

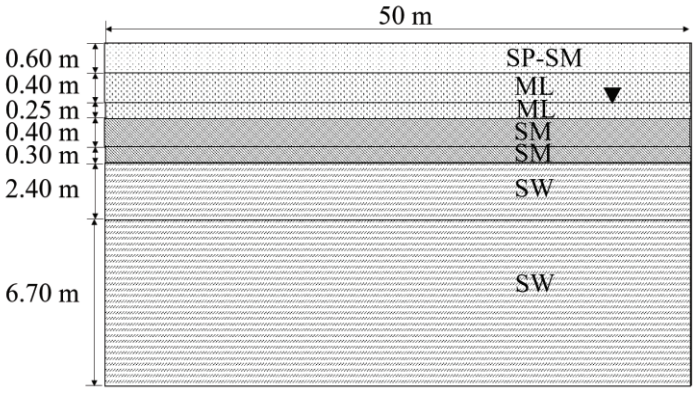

Figure 2. Soil profile

Table 1. Material properties of Natural, and Densified Soil (values in brackets if different from natural soil).

Layer	Depth Range (m)	Unit Weight (kN/m^3)	$N_{1,60}$	Shear Wave Velocity (m/s)	Shear Modulus (MPa)	*Shear Modulus Coefficient	*Relative Density	*Contraction Rate	Hydraulic Permeability (m/s)
SP-SM	0-0.5	17	15 [10]	102 [90]	18.2 [14.9]	699 [724]	0.73 [0.75]	0.77 [0.32]	$9x10^{-5}$
ML	0.5-1	17 [16]	10 [5]	102 [94]	18.0 [16.2]	590 [442]	0.50 [0.75]	0.38 [1.58]	$6x10^{-7}$
ML	1-1.25	17 [18]	5 [15]	98 [114]	16.6 [23.7]	467 [525]	0.33 [0.75]	0.93 [0.36]	$6x10^{-7}$
SM	1.25-1.75	17 [18]	5 [25]	105 [140]	19.2 [35.9]	457 [689]	0.33 [0.75]	0.93 [1.49]	$2x10^{-5}$
SM	1.75-2	19	10 [30]	119 [151]	27.6 [46.6]	590 [835]	0.44 [0.75]	0.57 [2.53]	$2x10^{-5}$
SW	2-3.25	19	10 [35]	150 [171]	43.4 [59.4]	590 [954]	0.42 [0.75]	0.64 [3.31]	$2x10^{-5}$
SW	3.25-10	19	20 [35]	155 [179]	46.7 [65.6]	792 [893]	0.66 [0.75]	0.38 [2.42]	$7x10^{-5}$

*PM4Sand required input parameters

Table 2. Material properties of RAP elements.

Depth Range (m)	Density kg/m3	Shear Wave Velocity (m/s)	Shear Modulus (MPa)	Bulk Modulus (MPa)	Poisson's Ratio	Hydraulic Permeability (m/s)
0-0.5	2039	555	628	5066	0.44	$7x10^{-5}$
0.5-1	2039	307	192	2840	0.47	$7x10^{-5}$
1-1.25	2039	217	96	1713	0.47	$7x10^{-5}$
1.25-1.75	2039	399	324	13870	0.49	$7x10^{-5}$
1.75-2	2039	574	673	34478	0.49	$7x10^{-5}$
2-4	2039	885	1598	64096	0.49	$7x10^{-5}$

RESULTS

This study separately measures co-seismic and post-seismic settlement. Co-seismic settlement corresponds to the rearrangement of soil particles during dynamic loading in unsaturated and saturated soil where the Δu are minimal (i.e., seismic compression). The post-seismic settlement is caused by the dissipation of Δu (i.e., consolidation). Accordingly, the results from the dynamic loading and consolidation stages are presented separately. The evolution of excess pore water pressure ratio (r_u) and strains are also discussed. Finally, note that all contour plots presented henceforth are limited to the center region of the model unless otherwise stated.

Dynamic loading

Excess pore water pressure

Figure 3 shows the computed distribution of r_u for all four models both with and without the application of the foundation load. As expected, r_u tends to increase in those layers with higher liquefaction potential as a result of dynamic loading. In particular, r_u reaches 85% in the silty sand layer (SM) located at depths from 1 to 2 m in natural conditions (Model 1) when the footing

is not loaded (Figure 3a left panel). Surficial evidence of liquefaction is expected for values of r_u this high in shallow layers, which is consistent with field observations after the CES (van Ballegooy et al. 2014; Wissmann et al. 2015). Smaller r_u values are predicted beneath the footing when it is loaded with 240 kPa (Figure 3a right panel), where the increased confining stress tends to stiffen the soil, thus limiting shear strain, and to some extent limiting the r_u generated. Finally, the inclusion of RAPs and densified zone are predicted to reduce r_u even further (Figures 3b, 3c, and 3d).

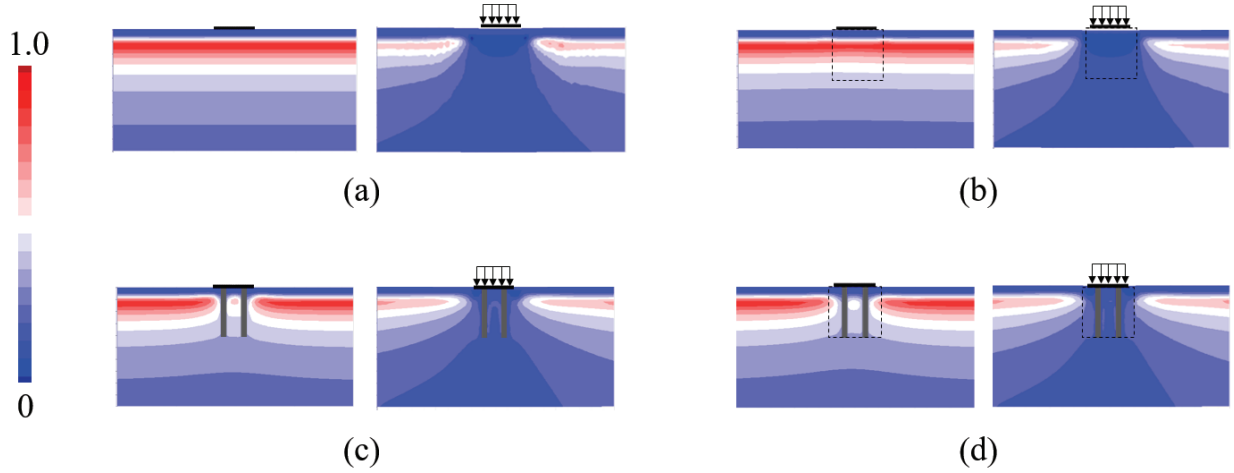

Figure 3. r_u contours at end of the dynamic loading for: (a) Model 1; (b) Model 2; (c) Model 3; and (d) Model 4. All models are analyzed with and without a load imposed on the footing.

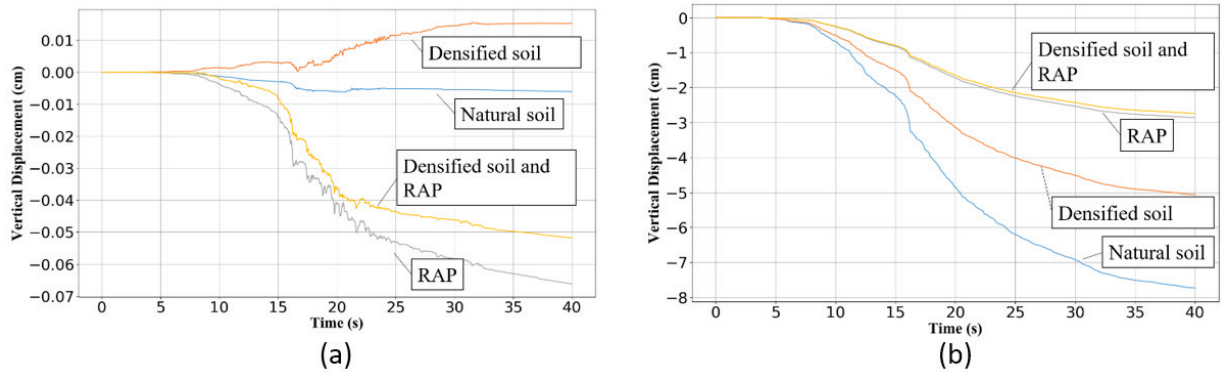

Figure 4. Vertical Displacement of the footing vs time for each model condition during dynamic loading for: (a) footing without load; and (b) footing with 240 kPa load.

Co-seismic settlement

The evolution of small but predicted co-seismic settlement values computed at the center of the footing is presented in Figure 4. When the footing is not loaded (Figure 4a), the model with the densified zone (Model 2) results in a heaving of the soil ~0.15 mm. For no-load conditions, the model that includes the RAPs but without densification predicts the largest settlements. All of the values are less than 1 mm. For models that include footing loads represented by a bearing pressure of 240 kPa (Figure 4b), predicted settlements range between approximately 7.5 mm for natural soil conditions (Model 1) to about 3 mm for both RAP without densification (Model 3)

and RAP with densification (Model 4) conditions. Figure 4b shows that the presence of the RAPs has greater benefit than the presence of densified soil. Figure 5a shows that for natural soil conditions, almost all of the settlement occurs in the soil within roughly the depth equal to one footing width from the footing bottom. In contrast, the models predict that the RAP reinforcement provides a more uniform settlement distribution with depth (Figures 5c and 5d for Models 3 and 4, respectively).

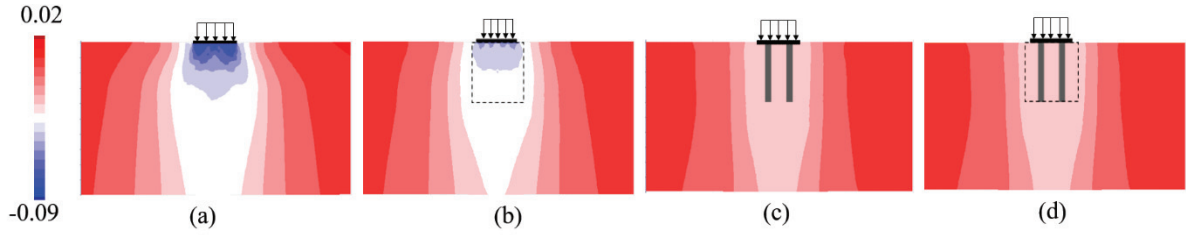

Figure 5. Vertical displacement at the end of the dynamic loading for footing with 240 kPa load: (a) Model 1; (b) Model 2; (c) Model 3; and (d) Model 4. Units in meters.

Shear and volumetric strains

Figure 6 shows different patterns of shear and volumetric strains for the various reinforcement conditions. For conditions where no foundation pressures are applied (Figure 6 left panels), shear strains are predicted to localize at depths between 1 and 2 m, coinciding with the liquefied soil layer (Figure 6a). For conditions including the footing load (Figure 6 right panels), the shear strains are predicted to concentrate below the edges of the unreinforced footing on the natural ground (Figure 6a), and to concentrate along the interface between natural soil and RAPs (or densified soil) and spread vertically downward (Figure 6b). In terms of volumetric strains induced by the loaded footings, the presence of the RAPs serves to change the distribution of maximum compression that is computed to be located immediately beneath the unreinforced footing on natural soil (Figure 7a) to between the base of the piers and also at the edges of the footing for reinforced conditions (Figure 7b).

Figure 8 presents the predicted shear and volumetric strain profiles down through the centerline of the model (Figure 8a) and 1 m to the right down through the centerline of the RAP (Figure 8b) for the loaded footing. Note that the shear strains within the RAPs are low because of their higher stiffness relative to the surrounding soil. Similarly, the volumetric strains are close to zero within the piers. Finally, the inclusion of RAPs clearly reduces the amount of shear and volumetric strains, even for conditions without densified soil.

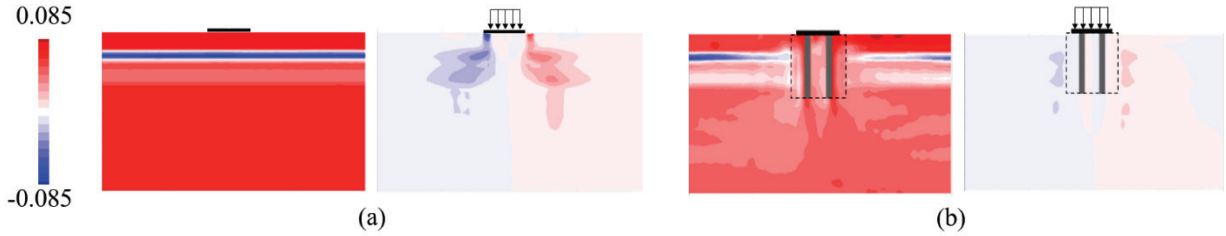

Figure 6. Shear strain at the end of dynamic loading for: (a) Model 1; and (b) Model 4. Results are shown for cases both with and without footing load.

Figure 7. Volumetric strain at end of dynamic loading for: (a) Model 1; and (b) Model 4. Results are shown for cases both with and without footing load.

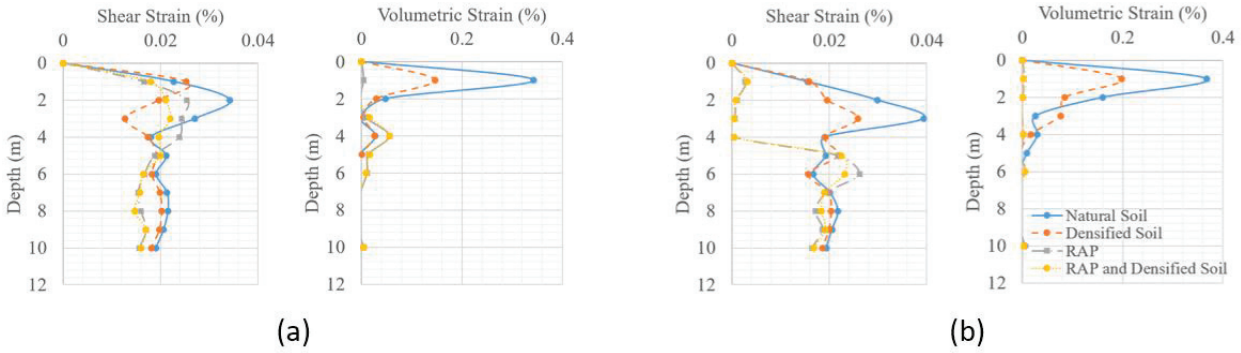

Figure 8: Distribution of shear and volumetric strains for vertical lines: (a) through the center of the model; and (b) 1 m to the right of the center of the model, down through the center of the RAP. Footing loaded with 240kPa.

Consolidation

Post-seismic settlement

Post-seismic consolidation settlement occurs when the excess pore water pressures generated during shaking dissipate. Figure 9 shows that the natural soil condition (Model 1) is predicted to have the largest vertical displacement, both when the footing is and is not loaded. This is followed by slightly reduced settlements predicted for densified conditions (Model 2). The predicted settlements are significantly less for the RAP reinforced conditions (Models 3 and 4), especially those in response to the loaded foundations where there is an approximate six-fold reduction in settlement. In terms of settlement distribution of loaded foundations, vertical displacements tend to be concentrated directly below the footings for natural and densified soil conditions (Models 1 and 2) consistent with a bearing capacity failure mechanism (Figures 10a and 10b right panels). Contrarily, when the footings are not loaded (Figure 10 left panels), the vertical displacements tend to be uniformly distributed laterally and decrease with depth (Figure 10a and 10b left panels). Finally, the settlements of loaded and not loaded footings that are reinforced by the RAPs (Models 3 and 4) accumulate on both sides of the footing beyond the RAPs and densified soil, and the settlements consistently decrease with depth (Figures 10c and 10d). Table 3 summarizes the post-seismic consolidation surface settlements.

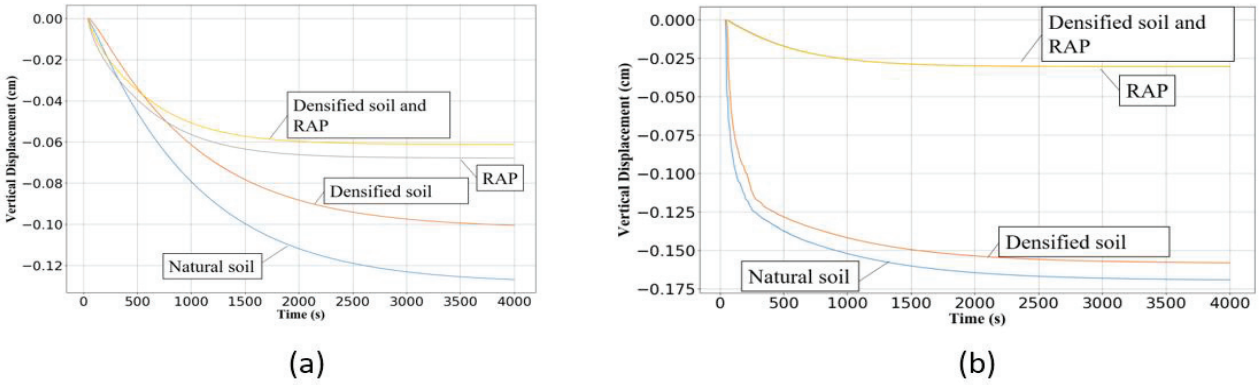

Figure 9. Post-shaking consolidation settlement as a function of time when: (a) the footings are not loaded, and (b) the footings are loaded.

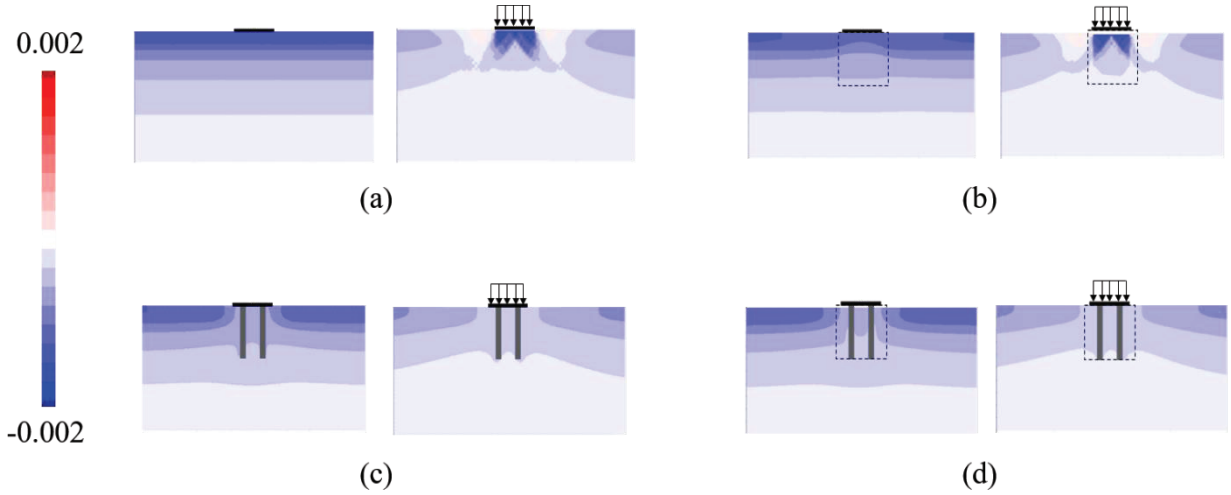

Figure 10. Vertical displacements at the end of post-shaking consolidation for models with and without footing load: (a) Model 1; (b) Model 2: (c) Model 3; and (d) Model 4. Units in meters.

Table 3. Co-seismic and post-seismic settlement predicted using the numerical simulations. The percentage of settlement reduction with respect to the natural soil (Model 1) is indicated in parentheses.

	Co-seismic settlement (cm)		Post-seismic settlement (cm)	
Model	**Footing not loaded**	**Loaded footing**	**Footing not loaded**	**Loaded footing**
1	0.005	7.5	0.13	0.17
2	-0.015	5.2 (31%)	0.10 (15%)	0.16 (6%)
3	0.065	2.7 (64%)	0.07 (46%)	0.03 (82%)
4	0.052	2.6 (65%)	0.06 (54%)	0.03 (82%)

CONCLUSIONS

The results of this work indicate that the inclusion of RAPs can significantly reduce the seismically-induced settlement of footings in liquefiable soils. The analysis is based on a set of fully-coupled hydro-mechanical models calibrated using extensive field test data collected from the GIP. When RAPs are included in the model, reductions of up to 64% are observed for the co-seismic settlement, and in the range of 54% to 82% for the post-seismic settlement. Additional observations resulting from including RAPs are: (a) the RAP-reinforced materials settle as a block and shear strain tends to localize at the edges between natural soil and ground improvement; (b) the existence of a zone with densified soil surrounding the RAPs does not play a significant role in settlement prediction; (c) RAPs help prevent shallow bearing capacity failure mechanisms from forming; (d) the liquefaction potential is reduced between the RAPs. Future work includes further studying the effects due to inertial loading from superstructure, the consideration of elastoplastic constitutive model for the RAPs¸ and the 3D effects.

ACKNOWLEDGMENT

This research was funded in part by Geopier Foundation Company and by the National Science Foundation (NSF) Grants CMMI-1825189 and CMMI-1937984. This support is gratefully acknowledged. However, any opinions, findings, and conclusions or recommendations expressed in this paper are those of the authors and do not necessarily reflect the views of the NSF or Geopier Foundation Company.

REFERENCES

Boulanger, R. W., and Ziotopoulou, K. (2017). PM4Sand (version 3.1): A sand plasticity model for earthquake engineering applications. Report No. UCD/CGM-17/01, Center for Geotechnical Modeling, Department of Civil and Environmental Engineering, University of California, Davis, CA, March, 73 pp.

Bradley, B. A. (2012). "Strong ground motion characteristics observed in the 4 September 2010 Darfield, New Zealand earthquake." *Soil Dynamics and Earthquake Engineering*, 42, 32–46.

Cubrinovski, M., and Green, R. A. (eds.). (2010). "Geotechnical Reconnaissance of the 2010 Darfield (Canterbury) Earthquake," (contributing authors in alphabetical order: J. Allen, S. Ashford, E. Bowman, B. Bradley, B. Cox, M. Cubrinovski, R. Green, T. Hutchinson, E. Kavazanjian, R. Orense, M. Pender, M. Quigley, and L. Wotherspoon), *Bulletin of the New Zealand Society for Earthquake Engineering*, 43(4), 243-320.

Cubrinovski, M., Bradley, B., Wotherspoon, L., Green, R. A., Bray, J., Wood, C., Pender, M., Allen, J., Bradshaw, A., Rix, G., Taylor, M., Robinson, K., Henderson, D., Giorgini, S., Ma, K., Winkley, A., Zupan, J., O'Rourke, T., DePascale, G., and Wells, D. (2011). "Geotechnical Aspects of the 22 February 2011 Christchurch Earthquake." *Bulletin of the New Zealand Society for Earthquake Engineering*, 44(4), 205-226.

Green, R. A., Maurer, B. W., and van Ballegooy, S. (2018). "The Influence of the Non-Liquefied Crust on the Severity of Surficial Liquefaction Manifestations: Case History from the 2016 Valentine's Day Earthquake in New Zealand." *Proc. Geotechnical Earthquake Engineering and Soil Dynamics V (GEESD V), Liquefaction Triggering, Consequences, and Mitigation* (S.J. Brandenberg and M.T. Manzari, eds.), ASCE Geotechnical Special Publication (GSP) 290, 21-32.

Ishihara, K. (1985). "Stability of natural deposits during earthquakes." *11th International Conference on Soil Mechanics and Foundation Engineering*. International Society for Soil Mechanics and Geotechnical Engineering, San Francisco.

Papadimitrious, A. G., Vytiniotis, A. C., Bouckovalas, G. D., and Bakas, G. J. (2006). "Equivalence between 2d and 3d numerical simulations of the seismic response of improved sites." *Proc., 8th U.S. National Conf. on Earthquake Engineering*, Oakland, CA, Earthquake Engineering Research Institute.

Thum, T. S., Yerro, A., Saade, A., Ye, E., Wissmann, K., and Green, R. A. (2021) "Numerical modeling of Rammed Aggregate Piers (RAP) in liquefiable soil." *Journal of Geotechnical and Geoenvironmental Engineering* (in preparation).

Tonkin and Taylor. (2015). *Residential Ground Improvement: Findings from trials to manage liquefaction vulnerability*. Wellington, New Zealand.

Roberts, J. N. (2017). *Field evaluation of large-scale, shallow ground improvements to mitigate liquefaction triggering*. Ph.D. Thesis, Department of Civil, Architectural, and Environmental Engineering, University of Texas, Austin, TX.

Saade, A. (2018). *Numerical Analysis of RAP Elements under Dynamic Loading*. MS Thesis, Department of Civil and Environmental Engineering, Virginia Tech, Blacksburg, VA.

Shahir, H., Pak, A., and Ayoubi, P. (2016). "A performance-based approach for design of ground densification to mitigate liquefaction." *Soil Dynamics and Earthquake Engineering*, Elsevier, 90, 381–394.

van Ballegooy, S., Cox, S. C., Thurlow, C., Rutter H. K., Harrington, G., Fraser, J., and Smith, T. (2014). Median water table elevation in Christchurch and surrounding area after the 4 September 2010 Darfield earthquake, Version 2. GNS Science Report 2014/18, Institute of Geological and Nuclear Sciences Limited, Lower Hutt, New Zealand, 79pp + appendices.

Wissmann, K. J., van Ballegooy, S., Metcalfe, B. C., Dismuke, J., and Anderson, C. (2015). "Rammed aggregate pier ground improvement as a liquefaction mitigation method in sandy and silty soils." *Proc., 6th International Conference on Earthquake Geotechnical Engineering*, ISSMGE, Christchurch, NZ.